# A new high-pressure mass spectrometer with improved reaction temperature measurement

Alexander Likholyot, Jamey K. Hovey, Terry M. Seward*

*Mass Spectrometry Laboratory, Geochemistry Group, Institut für Mineralogie und Petrographie, ETH-Zentrum (Swiss Federal Institute of Technology), CH-8092 Zurich, Switzerland*

## Abstract

The high-pressure mass spectrometric technique (HPMS) can provide detailed gas-phase thermochemical data including free energies, enthalpies, and entropies for various ion-molecule reactions. Several problems related to accuracy of the HPMS method have been previously identified. These problems in addition to accuracy of ion source temperature measurement and control were considered in our attempt to construct an overall HPMS experiment that would lead to an improved accuracy in the derived thermochemical data. Design of the new ion source together with other construction details of our HPMS apparatus are described in this paper. The performance of the newly constructed high-pressure mass spectrometer was evaluated by studying the thermochemistry of stepwise hydration of chlorine anion in the gas-phase. Density functional theory calculations were performed to aid in choosing appropriate experimental conditions. The experimental and theoretical results exhibit non-monotonic trends in stepwise enthalpies and entropies of chloride ion hydration that are in disagreement with the results of previous HPMS studies. Detailed analysis of HPMS experimental errors is given in an attempt to explain the discrepancies.
© 2004 Elsevier B.V. All rights reserved.

*Keywords:* High-pressure mass spectrometry; HPMS; Chloride; Hydration

## 1. Introduction

A detailed knowledge of the fundamental manner in which ions and molecules are solvated in aqueous media is required for an understanding of numerous natural processes. Ion-molecule clustering reactions in the gas phase are direct analogs to ionic solvation in a fluid. In addition, the thermochemistry of stepwise solvation reactions can be used directly in the construction of solvation theories and in the development of interaction potentials for molecular dynamics simulations. The high-pressure mass spectrometric technique (HPMS) can provide accurate gas-phase thermochemical data including free energies, enthalpies, and entropies for various ion-molecule reactions. A number of previously identified problems in the use of HPMS to generate accurate thermochemical data have been considered in this attempt to

construct an HPMS apparatus that would potentially generate the most accurate thermochemical quantities to date.

The pulsed-electron high-pressure mass spectrometric technique was originally developed by Paul Kebarle and coworkers using alpha-particle sources in the 1960s and settled into a successful workable design in the early 1970s with continual improvements in the following years. A comprehensive introduction to HPMS and the history of its development is given in Ref. [1]. Our implementation of the HPMS technique explicitly builds upon other successful designs from the groups of Hiraoka et al. [2] and McMahon and coworkers [3]. Several areas of potentially important improvement were identified in these early instruments centered mostly on the ability to unambiguously define the temperature in the reaction chamber. A simple analysis of errors associated with quantities such as the change in enthalpy and entropy that are implicitly derived via derivatives of measured ionic ratios with respect to temperature is given in the following sections. It is shown that strict knowledge and control of

* Corresponding author. Tel.: +41 1 632 22 27/8; fax: +41 1 632 10 88.
  *E-mail address:* tseward@erdw.ethz.ch (T.M. Seward).

temperature is required in order to obtain even reasonably accurate values for these quantities. Kebarle and Hiraoka [4] noted the importance of a sufficiently high vacuum in the source chamber to minimize undesirable competing reactions, including collision-induced dissociation (CID). The current implementation of the HPMS technique was developed with these and other concerns in mind.

## 2. Construction details of HPMS apparatus

### 2.1. Overall layout of the HPMS experiment

The overall layout of our HPMS setup is shown in Fig. 1. Samples are prepared in the gas-handling plant by injecting the gas(es) or liquid(s) of interest with a calibrated syringe into a 5 L glass mixing bulb containing a carrier gas, generally methane. After sufficient equilibration time, the mixture is allowed to flow through the ion source. Alternatively, liquid samples may be introduced directly into the controlled methane flow with a syringe pump fitted through a septum port. This method is less accurate in terms of known sample concentrations in methane, but is easier to use. Ions are produced in the high-pressure ion source by a 4 kV electron beam irradiation. The physical conditions and behavior of ions in the ion source are considered in detail in Ref. [5]. The ion source is floated to a potential of 4 kV. A small fraction of ions escape from the ion source through an ion exit slit, undergo 4 kV acceleration and then enter the mass analysis section of the mass spectrometer.

The ions first enter the electrostatic analyzer (ESA) that performs energy filtering. Following the ESA, the monoenergetic ion beam enters the magnetic field that performs momentum filtering. Ions are detected by electron multipliers. The fitted analog multiplier outputs a signal proportional to the impeding ion current and the digital multiplier outputs pulses proportional to each detected ion, thus allowing for discrete ion counting. The analog multiplier is used to acquire overall mass spectra, whereas the digital multiplier is used in pulsing experiments to follow reaction kinetics and the approach to equilibrium.

Equilibrium studies were performed in the pulsing mode of operation. The electron beam is gated by short pulses from a master pulse generator through an optically isolated floating pulse amplifier. The electron beam pulse width is generally kept between 3 and 50 μs and the pulse period between 1 and 50 ms. Ions are formed after each electron pulse and undergo various chemical reactions in addition to ionic diffusion to the ion source walls whereupon they discharge. Ions that escape from the ion source through the ion exit slit are selectively mass-filtered by the mass analysis section of the mass spectrometer set to monitor a specific mass of interest. Within a preset fixed mass window, only ions of this mass are detected by the digital electron multiplier. The output of the multiplier is fed after preamplification into a multichannel scaler. The multichannel scaler is synchronized with the electron beam pulse via the master pulse generator and records ion counts as a function of time after each pulse. This recording is achieved by counting ions for discrete periods of time (∼1–20 μs time channels) and performing this operation over a sufficiently
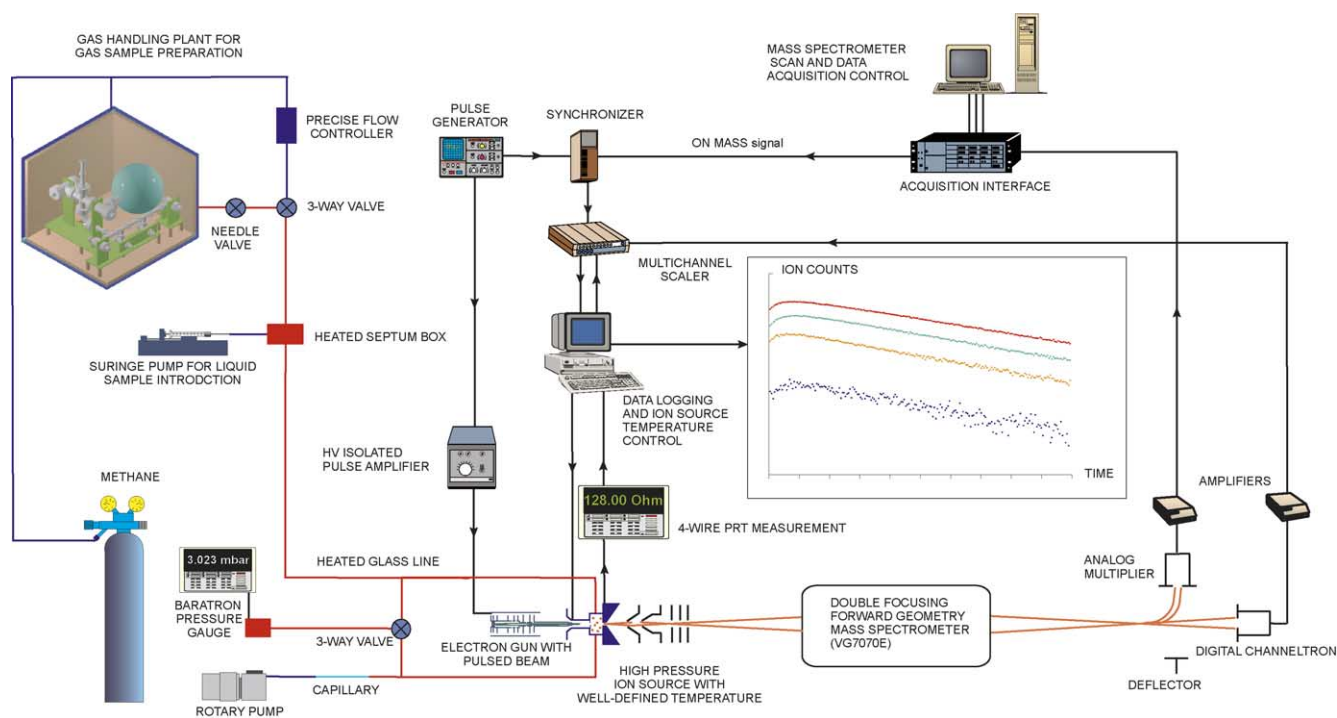


Fig. 1. The overall experimental setup.

large number of channels. The pulsing sequence is performed several thousand times to accumulate enough ion counts in each time channel and for improvement of the signal-to-noise ratio.

The detected ion signal at any time is proportional to the number density of ions of a given mass in the ion source. The concentrations of different ions in the source can be recorded as a function of time to within a machine-dependent factor. If two ions are monitored, the ratio of recorded ion counts will yield the ratio of ion concentrations in the source as a function of time under the assumption that the machine-dependent factor is the same for ions of different masses. This assumption does not always hold and the factor might be mass dependent in certain cases, such as when mass discrimination is present due to molecular outflow from the source exit slit [5].

The data collection part of the experiment is fully automated by synchronizing the ion detection subsystem with the existing mass scan facilities and data system of the mass spectrometer. The mass spectrometer data system and the magnet are programmed to monitor a given list of ionic masses, each for a fixed period of time during which the multichannel scaler records time profile for that mass. After all the masses from the list have been recorded, this sequence is repeated again. In this manner, the mass spectrometer switches between masses of interest several times during the total period of time needed to accumulate sufficient signals. As a result, several time profiles are available for each mass. By averaging these profiles for each mass, any effects of potential changes in the conditions inside the ion source during the course of the measurement are greatly reduced compared to the case when each mass is recorded only once, but over a longer period of time. Details of the construction of various components are given in the following sections.

### 2.2. Modifications to the commercial mass spectrometer

The new HPMS apparatus was constructed using an existing VG 7070E magnetic sector double-focusing mass spectrometer of EB geometry. A magnetic sector machine was acquired preferentially over a quadrupole instrument to minimize problems due to mass dependent sensitivity. Modifications were made to the overall pumping speed in the source housing as well as to some ion optics and the ion detection system.

The commercial VG 7070E spectrometer is pumped by two Edwards diffusion pumps in the source and analyzer regions, respectively. The original Edwards 160/700M source diffusion pump (700 L/s of N2) is connected to the source chamber by a 142 mm i.d. stainless steel tube. Because of the high pressures involved with the HPMS experiment, it was necessary to add a Leybold TMP1000 (1150 L/s of $N_2$) ceramic bearing turbo pump mounted directly above the ion-exit slit in a vertically inverted position. The 250 mm "conflat" pump flange (CF) from the turbo pump was mounted onto a thick stainless steel adapter connected between a mating 250 mm CF flange and a 152 mm × 102 mm rectangular slot cut into the top of the commercial source chamber. The conservation of cross-sectional area in this adapter has minimized conductance losses due to the adapter. The original source flange was replaced by a flange assembly that also incorporates an electron gun mount and appropriate electron gun housing chamber. The original source chamber was expanded to accommodate this larger assembly. The electron gun chamber is differentially pumped with an Edwards 63/150M diffusion pump (135 L/s of $N_2$). The turbo pump is only used during the course of experimental measurements, and the ultimate vacuum of this system is better than $4 \times 10^{-7}$ mbar after an appropriate bakeout. Several large (Edwards E2M40, 2xE2M28) roughing pumps were added to the source high vacuum pumps. In this configuration, there is differential pumping of the analyzer, electron gun, and ion source regions. As such, a vacuum of better than $5 \times 10^{-7}$ mbar is maintained during an experiment in the analyzer and $5 \times 10^{-6}$ mbar in the electron gun regions leading to a pressure in the source chamber not exceeding $5 \times 10^{-5}$ mbar for the source pressures employed to date.

It was found that the original Y (horizontal plane perpendicular to ion beam) and Z (vertical plane) focusing and deflection was responsible for a loss in ion sensitivity due to losses in the region prior to the ESA. We have therefore added a series of precision-machined stainless steel plate lenses in the first field-free region prior to the ESA and have achieved increased ion sensitivity by nearly a factor of 2. In addition, the possibility of digital signal acquisition was added by expanding the ion detection region and placing a Galileo Channeltron 4870V electron multiplier at exactly the same position as the existing analog conventional electron multiplier.

### 2.3. High-pressure ion source and electron gun

The HPMS ion source consists of an electron gun mounted coaxially to the produced ion beam and the high-pressure source itself and is shown schematically in Fig. 2. Because the VG 7070E mass spectrometer is capable of operating with 6 kV of ion acceleration potential, the electron gun was designed to operate with the filament floated at −12 kV. This large potential would be required if 6 kV of electron acceleration was to be used for the highest ion acceleration (negative ions). Design of the electron gun was based on previous versions of electron guns from Kebarle [1], Szulejko et al. [6], and by examination of 3–4 kV cathode ray tubes used in a variety of well-focused Hewlett-Packard oscilloscopes. The initial design was simulated using the ion optics software package SIMION [7] and the final version of the electron gun capable of providing 2–6 kV of acceleration for positive ions (starting at ground potential) or negative ions (starting at a potential below ground) was constructed. The electron gun was powered by a custom-built filament power supply (QVR Designs LLC) capable of floating to ±15 kV and a precision high voltage divider. Conventional VG 7070E filaments were

**Detailed diagram of the combined pulsed-electron gun and high-pressure ion source.**
(1) Electron mount flange containing 16 electrical feedthroughs; (2) electron gun housing equipped with port to Edwards 63/150M diffusion pump (bottom flange); (3) MACOR ceramic electron gun mount; (4) stainless steel mount; (5) additional ceramic spacers for high voltage protection; (6) ion-gauge port; (7) viewport flange; (8) VG 7070E filament; (9) Filament mount plate; (10) drawout electrode; (11) Einzel lens 1; (12) Einzel lens 2; (13) Einzel lens 3; (14) deflect A; (15) deflect B; (16) electron exit cone; (17) ceramic tube; (18) high-pressure source flange containing 28 feedthroughs, 2 ceramic breaks used in gas inlet/outlet lines, and 2 Cajon fittings used in cooling assembly; (19) original source housing; (20) MACOR ceramic source mount; (21) stainless steel stabilizing mount ring; (22) copper ring with embedded 1/8 inch stainless steel tubing used for cooling; (23) stainless steel source mount ring; (24) main copper source block encasing the source spool and containing 8 cartridge heaters (Chromalox) and auxiliary PRT used for temperature monitor or control; (25) the main high-pressure source volume of 1 mL; (26) electron beam entrance orifice (100 micron dia); (27) 1/8 inch stainless steel gas in/out lines; (28) stainless steel cup for main monitor and control PRT; (29) ion-exit slit (10 micron x 1mm); (30) copper ion-exit thermostatter equipped with monitor thermocouple; (31) heated and temperature controlled copper adiabatic shield; (32) stainless steel heat shield; (33) 4 mounting rods wrapped with stainless steel wire to form cylindrical field free region; (34) ion extraction cone 1; (35) ion extraction cone 2; (36) beam focussing/centering plates; (37) original VG plate; (38) original VG adjustable ion exit slits; (39) location of 6 inch diffusion pump; (40) location of 250mm turbo pump.

Fig. 2. The HPMS ion source and electron gun.

used as obtained from VG Micromass or Haltech Inc. Initial tests of the electron gun for optimum voltage characteristics were performed using a phosphor screen obtained from Kimball Physics Inc. and showed that the resultant electron beam was stable and relatively tightly focused. The position of the electron gun can be clearly seen in Fig. 2. The electron gun is fixed to a stainless steel mount (4) that is electrically isolated by four ceramic spacers from the electron gun filament mount plate (7) and from the electron gun feed-through flange (1) by a 25 mm machineable ceramic (MACOR) mount. The electron gun was mounted in-line with the high-pressure source as guided through the electron gun housing (2) through a ceramic guide (18) that also serves as a differential pumping aperture. Voltages were provided by high-voltage (20 kV) feed-throughs mounted on the main electron gun flange (1). The electron gun and its housing were designed such that the filament could be replaced without completely removing the high-pressure source from the mass spectrometer or disassembling the electron gun. The electron gun housing was equipped with a viewport for visual confirmation of filament power or to check for potential high voltage breakdown. The electron beam was shielded from magnetic fields by 0.1 mm thick mu-foil (Magnetic Shield Corp.) wrapped in three layers around the ceramic tube (17), the electron exit cone (16), and inside the cylindrical channel located in the center of

the copper source block (24). No observable effect of the mass spectrometer magnet on the electron beam focusing and deflection conditions was detected. This is an important requirement because the number of electrons entering the ion source after each electron beam pulse must be independent of the mass monitored by the mass spectrometer.

As outlined previously, one of the main goals during the construction of this new HPMS ion source was to minimize errors due to temperature instability or lack of precision in its measurement. As such, the design was based partly on successful high-temperature calorimeters that maintain temperature stability to better than $10^{-3}$ K [8]. The central component of the ion source is the stainless steel source "spool" (25) that was constructed from 10 mm o.d. and 0.5 mm wall thickness tubing and had an internal volume of approximately 1 cm$^3$. A thin-walled 2 mm i.d. stainless steel cup inset into the spool was fitted to house the main platinum resistance thermometer (PRT). Two 1/8 in. stainless steel gas inlet and outlet lines were also welded to the source spool as shown in Fig. 3. This internal ion source chamber is sealed using a scaled-down version of the NW16 CF flange and gold-plated copper gaskets. Ion exit and electron entrance apertures were constructed using a standard stainless steel orifice (100 μm diameter for electron entrance) and slit (10 μm × 1 mm for ion exit) obtained from Melles Griot,
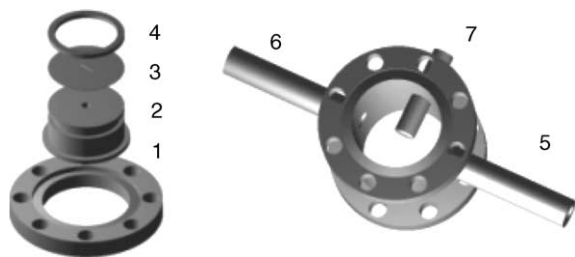
Fig. 3. The ion source spool and flange; the ion exit and electron entrance flanges are of identical design; the height of cylinder (2) welded to the flange (1) determines the volume of ion source; standard foil with circular or rectangular orifice (3) is sandwiched between cylinder (2) and washer (4) and welded along the outside edge; the gas inlet and outlet lines (5, 6) and main PRT cup (7) are welded to the source spool; the PRT cup has the end inside the source blanked.

that were welded onto the source flanges. The entire source spool sits tightly encased in a large nickel-plated copper source block machined to an extremely high tolerance so as to maintain good thermal contact between the source spool and the block. The gas lines are sandwiched tightly into the large copper source block for temperature pre-equilibration and are, in turn, connected to high voltage ceramic breaks (6 kV, Kurt Lesker Company) and to 1/4 in. high-voltage stainless steel isolated feed-throughs (12 kV, Kurt Lesker Company) that were welded to the source flange (18) as shown in Fig. 2. Silver solder used in the construction of the ceramic breaks limited the experimentally usable maximum temperature to approximately 600 °C. The thin source spool, large copper block, and inset PRT element were all designed to minimize temperature gradients near the source, provide temperature uniformity, and ultimately to provide accurate knowledge of the temperature of the reaction during the course of the experimental measurements. The copper block was fitted with eight cartridge heaters (Chromalox, CIR type) and various control and monitoring (PRT and thermocouple) temperature elements. A thick copper ion-exit plate (30) was used to maintain thermal contact near the ion-exit region and was fitted with a monitor thermocouple. The entire source block was enveloped by a 4 mm thick nickel-plated adiabatic copper shield embedded with a 1 mm o.d. Omegaclad metal-sheathed thermocouple wire (Omega Engineering) used as a heater. The adiabatic shield had an embedded monitor thermocouple that was used together with a Eurotherm temperature controller to maintain a preset temperature. The shield was located such as to maintain a 5 mm gap between the source block and the shield. This shield, in turn, was surrounded by an unheated nickel-plated stainless steel tube used as an outer heat shield. This combination of adiabatic shield and outer heat shield minimizes radial radiative heat losses and provides excellent temperature stability and uniformity. Even when no heating or temperature control of the adiabatic shield was used, the temperature stability was found to be no worse than 0.02 °C RMS (root mean square) over 1 h throughout the entire temperature range used (−45 to 540 °C). For

the most common temperature range (30–200 °C), the stability was better than 0.001 °C RMS over one hour.

Ions exit the high-pressure source and enter the cylindrically shaped field-free region constructed using four stainless steel rods (33) wrapped concentrically using 0.8 mm stainless steel wire with spacing of 3–4 mm between the loops. The first ion extraction cone (mirror polished to reduce radiative heat losses) incorporating a 4 mm opening was fixed to the source via four stainless steel rods and was electrically isolated using ceramic spacers. A second cone containing a 3 mm opening was mounted between this and the ion focus and deflection plates (36, 37). The VG 7070E adjustable source slit (38) was retained although normal operation was achieved when the slit was fully open that yielded an instrument resolution of approximately 500–1000. The entire source is mounted onto an original VG 7070E source flange using a stabilizing stainless steel ring source mount assembly (21, 23) held together by four stainless steel rods and designed to minimize stress on the main ceramic isolating mount (20). This source mount was fitted with a cooling assembly constructed using 1/8"stainless steel tubing sandwiched inside in a copper ring and tightly fixed to four rods on the source mount. The tubing is electrically isolated from the flange using two 1/4 in. Cajon glass-to-metal adapters. The ion source can be easily cooled to −100 °C by flowing cold nitrogen gas through the cooling assembly. The gas is cooled by passing it through a copper coil immersed in liquid nitrogen. The source flange is equipped in total with 28 electrical feed-throughs in addition to two high-voltage gas feed-throughs connected to the gas inlet and outlet lines and two Cajon fittings for the cooling assembly.

A Minco S274PD type PRT was used for ion source temperature measurement. These PRTs are encased in a ceramic capsule 2 mm in diameter and 10 mm long. A four-wire resistance measurement was performed for temperature determination. A four-wire measurement ensures that lead resistances cancel. Nichrome wire was used for the lead extensions that were spot-welded to the original platinum PRT leads 8 mm away from the PRT body. Nichrome has a thermal conductivity 2.5 times lower than platinum and 30 times lower than that of copper. This choice of wire was dictated by the desire to reduce temperature measurement errors that might occur when using wires with higher thermal conductivity. Heat may be pumped away from the light platinum sensor in the PRT through lead wires if they are at a temperature lower than the PRT when lead extensions have a sufficiently high thermal conductivity. Approximately 12 cm of the Nichrome lead extensions were placed in four-hole ceramic capillaries and were mounted in the copper block (24) to ensure good thermal contact with the block.

Prior to being mounted in the ion source, the PRT was calibrated against a NIST traceable secondary reference standard PRT in a specially designed calibration vessel. The main part of the vessel was a copper cylinder 25 mm in diameter and 150 mm long. The secondary reference standard PRT was placed in the channel in the center of the cylinder and the source PRT was placed in another channel immediately ad-

jacent to it. Metal-sheathed Omegaclad thermocouple wire was wrapped around the cylinder and was used as a heater. The cylinder was placed inside a polished stainless-steel tube that served as a heat shield, similar to our ion source design. The whole assembly was placed inside an evacuated stainless steel manifold. The mounting of the copper cylinder inside the shield and the shield inside the manifold was done using sharpened pins to have only point contacts to reduce conductive heat losses. The calibration was performed over the temperature range 30–470 °C and PRT coefficients were calculated following the NIST guidelines given in Ref. [9]. For temperatures below 30 °C, the calibration was extrapolated. According to Ref. [9], most PRTs have an error of a few mK when the calibration is extrapolated in this manner which is negligible in our case. The accuracy of the present calibration was estimated to be 0.05 °C. The calibration of the secondary reference standard PRT was rechecked by an external calibration laboratory after the calibration of the ion source PRT and was found to be consistent with its original calibration.

The four-wire resistance measurement of the source PRT was performed by a Keithley 2001 Multimeter floated at the ion source potential and powered through isolation transformers. The data were sent to a monitoring computer via an optically isolated IEEE bus. The computer facilitated the conversion of resistance to temperature and implemented a PID algorithm for the ion source temperature control. Control of the ion source heaters was of the time-proportioning type. The computer output pulses of variable width to control the heater power. The pulses were sent via a fibre-optic link to a solid-state relay floated at the ion source potential that switched the source heaters on and off.

### 2.4. Sample introduction system and pressure measurement

The gas handling plant (GHP) consisted of a stainless steel manifold with all-metal valves and a 5 L glass bulb fitted with a septum inlet port. The exact volume of the bulb was calibrated using water. The manifold and bulb were mounted inside a uniformly heated box. The temperature inside the GHP was kept at 140 °C and was controlled by a temperature controller using a thermocouple sensor. The pressure in the GHP was measured using a 1000 mbar MKS Baratron 628A absolute pressure transducer.

Gas lines from the GHP to the ion source and from the ion source to the outlet rotary pump were constructed of 2 m long glass tubes having a 9 mm inside diameter. Small segments of the lines immediately adjacent to the source (~60 cm length) were made from glass tubes having a 4 mm inside diameter. This length of glass tube was chosen to avoid electrical breakdown through the gas from the ion source to ground when maintaining low ion source pressures. These glass lines were designed to operate at the ion source potentials of up to 6 kV. For comparison, HPMS machines in the laboratory of Kebarle [1] had 60 cm long glass lines for ion source operating voltages of up to 2 kV. The glass lines were wrapped

with tape heaters and were kept at 140 °C by temperature controllers. The glass tubes were connected together using stainless steel or Teflon Swagelok-type unions with Teflon ferrules. The Teflon unions were drilled through in order to minimize the surface area of Teflon exposed to the gas flow. The flow from the GHP was regulated by means of a Hoke MilliMite 1300 stainless steel metering valve. When the syringe pump was used for sample introduction, the methane flow was controlled by an MKS 1679A Mass-Flo flow controller.

The pressure was measured at the far ends of the 2 m glass lines by a 10 mbar MKS Baratron 628A absolute pressure transducer, which could monitor either inlet or outlet line pressures and was switched by means of a Hoke SelectoMite 7165 stainless steel three-way valve. Because we were not able to measure the pressure directly in the ion source, we ensured that the inlet and outlet gas lines were identical. In addition, the combined conductance of the gas lines from the points of pressure measurement to the ion source and conductance of the ion exit and electron entrance slits in the ion source was measured as a function of source temperature. This was achieved by alternatively closing off either inlet or outlet line and measuring the gas flow through the ion source using a calibrated flow meter and monitoring pressures at the ends of both lines. With such an arrangement, one of the pressures will be equal to the pressure inside the ion source. The obtained calibration data were used to calculate the corresponding pressure in the ion source in the normal flow-through configuration from measured pressures at the ends of the inlet and outlet lines. The ratio of inlet to outlet pressure was in the range 1.5–2.3 when ion source temperature ranged from −45 to 170 °C, respectively. The accuracy of this conductance calibration was found to be no worse than 0.05 mbar in ion source pressure. The partial pressure of a sample in the ion source was calculated from the known GHP total bulb volume, the volume of injected sample, the pressure and temperature of methane in the GHP before injection, and the total pressure inside the source. When the syringe pump was used, the partial pressure was calculated from the known syringe pump injection rate, the known methane flow rate, and the total pressure inside the ion source.

## 3. Experimental

Reactions of stepwise hydration of chloride (1) were chosen for evaluation of performance of the HPMS apparatus since there have been a number of previous investigations of the thermodynamics of chloride hydration using HPMS [10–12].

$$Cl^-(H_2O)_{n-1} = Cl^-(H_2O)_n \tag{1}$$
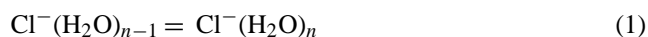
where $n = 6$ in Ref. [10] and $n = 4$ in Refs. [11,12]. Enthalpy for an additional hydration step beyond the experimentally determined steps mentioned above was estimated in Ref. [10] using an assumed value for the entropy change and experi-

mental values for the free energy change determined at one or two temperatures. All of the previous investigations used ion sources based upon the original Kebarle designs and similar to the one used in Ref. [12]. The results obtained in these studies are in rather good agreement. We have tried to further extend the range of experimentally observed cluster sizes for $Cl^-$ and the number of hydration steps measured under equilibrium conditions using our newly constructed ion source which we consider to be an improved design.

The samples were prepared in the gas handling plant by injecting distilled water containing traces of $CCl_4$ (0.5 vol.%) with a microliter syringe into a 5 L gas mixing glass bulb kept at 140 °C and filled with methane. After an equilibration period of ∼20 min, the mixture was allowed to flow from the bulb through the ion source. Water partial pressures in the source were generally in the range 0.02–0.35 mbar. Halide ions are formed by dissociative electron capture from $CCl_4$. Exothermic association reactions of the type described by Eq. (1) require third-body collisions for removal of the excess energy from the initially excited products. Following an electron pulse, ions diffuse to the walls through the major neutral component at the same time engaging in the following reaction:

$$Cl^-(H_2O)_{n-1} + H_2O + CH_4 = Cl^-(H_2O)_n + CH_4 \qquad (2)$$
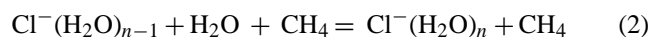
In addition to being a third-body agent in this reaction, methane also serves to thermalize the electrons and trap the ions in the ion source. It is important to elaborate on the ion source pressure range for best operation of the HPMS technique. Equilibrium HPMS studies require that ion residence times in the ion source are longer than equilibrium establishment times. This is achieved by trapping ions in the ion source for a time sufficient to establish equilibrium for reaction (2) with sufficiently high pressures of a carrier/buffer gas. However, if the ion source pressures are too high, then acceleration of the ions following escape from the ion source might lead to collisional dissociation through collisions with neutral gas molecules that have also escaped from the ion source. Acceleration voltages as low as 1–3 V may supply enough energy for collisional breakup. To remedy this situation, the pressures in the ion source at any given source temperature should be kept sufficiently low, yet high enough to observe equilibrium. As a general rule, the gas number density in the ion source was kept constant throughout the experimental temperature range. This meant having progressively lower pressures in the ion source at lower temperatures. Fig. 4 shows our experimental pressures which were employed at different temperatures. With this HPMS instrument's gas lines and source slits conductances, methane flow rates in the range 1.5–5 standard $cm^3$/min were required to realize such pressures.

Ionizing electron pulse widths of 5–70 μs and electron gun filament currents of 4–5 A were employed. It is undesirable to deliver too many electrons to the ion source since the resulting ionic profiles may display several changes of slope,
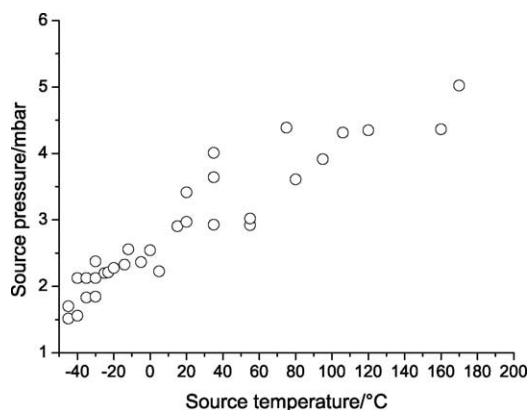


Fig. 4. Experimentally employed ion source pressures at different ion source temperatures.

as discussed in [5] and are somewhat difficult to analyze. The time between electron pulses was normally adjusted to 13–20 ms. This time was, in general, chosen to be three times longer than the ion residence time in the ion source that could be evaluated from ionic profiles (2–5 ms). It might be argued that a fraction of the ions might still remain in the source at times longer than the estimated residence time, which would lead to erroneous results. However, the equilibrium ionic ratio is determined from detected ion counts and any ion currents that are below the inherent detection limit should not change it to any significant extent. Tests with time periods varying up to 50 ms were carried out and yielded identical results to the shorter times periods. The multichannel scaler channel dwell-time was normally set to 10 μs and the reactions were monitored for 5–10 ms. Between 2 and 10,000 pulses were sufficient to obtain reasonable ionic profiles. Data acquisition was performed in a programmed mode. Each ion was monitored for ∼30 s in succession and then this sequence was repeated several times. Comparison of several profiles for each ion allowed assessment of the overall stability of conditions in the ion source during the course of the experiment.

At low ion source pressures, the reactants and products may be assumed to behave as perfect gases. For a standard state pressure of 1000 mbar the equilibrium constant for reaction (1) is given by,

$$K_n = \frac{I_n \times 1000}{I_{n-1} \times p(H_2O)} \qquad (3)$$

where $p(H_2O)$ is the water partial pressure, and $I_n$ and $I_{n-1}$ are measured intensities of $Cl^-(H_2O)_n$ and $Cl^-(H_2O)_{n-1}$, respectively, after equilibrium has been established. The ratio of measured ionic intensities should remain constant when equilibrium conditions apply. Once the equilibrium constants at several temperatures are determined, the enthalpy and entropy changes for the reaction (1) can be calculated from plots of the logarithm of equilibrium constant against reciprocal temperature as defined by the van't Hoff isochore,

$$\ln K = -\frac{\Delta H^\circ}{R}\left(\frac{1}{T}\right) + \left(\frac{\Delta S^\circ}{R}\right) \qquad (4)$$

If the van't Hoff plots exhibit linearity, as was the case for studied clustering reactions, then the enthalpy and entropy changes are easily obtained from the slopes and y-intercepts.

The various experiments were performed over a temperature range $+170\,°C$ to $-45\,°C$. This lower temperature limit was a result of the saturated water vapor pressure becoming too low as a result of some water vapor condensation inside the ion source.

## 4. Calculations

To aid in choosing appropriate experimental conditions, density functional theory (DFT) calculations have been performed on all studied chloride water clusters. Full geometry optimizations and frequency calculations were performed with the hybrid B3LYP method using GAUSSIAN98 [13] software. The Cl, H, and O atoms were described using GAUSSIAN98's built-in 6-311++G** basis set which includes polarization and diffuse functions. Starting with $n = 2$, two distinct geometry types were considered for each of the halides: one with the anion surrounded by water molecules, corresponding to interior solvation (I) and the other with the anion bound to the surface of a water cluster, corresponding to surface solvation (S). We considered one isomer of each type (surface and interior) for each cluster size. Structures similar to those reported by previous investigations [14–16] were used as starting geometries for the optimizations. Subsequent frequency calculations were used to verify

that a resultant optimized structure was indeed a minimum on the potential energy surface and to obtain thermochemical information as a function of temperature. All frequencies were scaled using a common factor of 0.89. Use of a scaling factor of 1.0 does not change calculated enthalpies and entropies for stepwise hydration reactions significantly. Typical changes for enthalpy and entropy are only $0.8\,\text{kJ mol}^{-1}$ and $2\,\text{J mol}^{-1}\,\text{K}^{-1}$, whereas typical experimental uncertainties are $2\,\text{kJ mol}^{-1}$ and $4\,\text{J mol}^{-1}\,\text{K}^{-1}$, respectively. Results of DFT calculations were used to explore the stability of clusters under different temperatures. Experimental temperature ranges for each stepwise hydration reaction (1) were chosen such that only negligible fractions of all involved clusters were excited above dissociation threshold within and could undergo unimolecular dissociation during mass analysis within that temperature range.

## 5. Results and discussion

Typical ionic profiles are shown in Fig. 5. It can be seen that 0.6 ms after the electron beam pulse, the profiles become parallel and equilibrium is probably established. The overall decay in ionic intensities is caused by loss of ions through diffusion to the ion source walls and consecutive discharge. A more convenient examination of the profiles results when individual ionic intensities are normalized to the total ion intensity [17]. Normalized profiles for a representative system are shown in Fig. 6. It can be seen that the profiles become
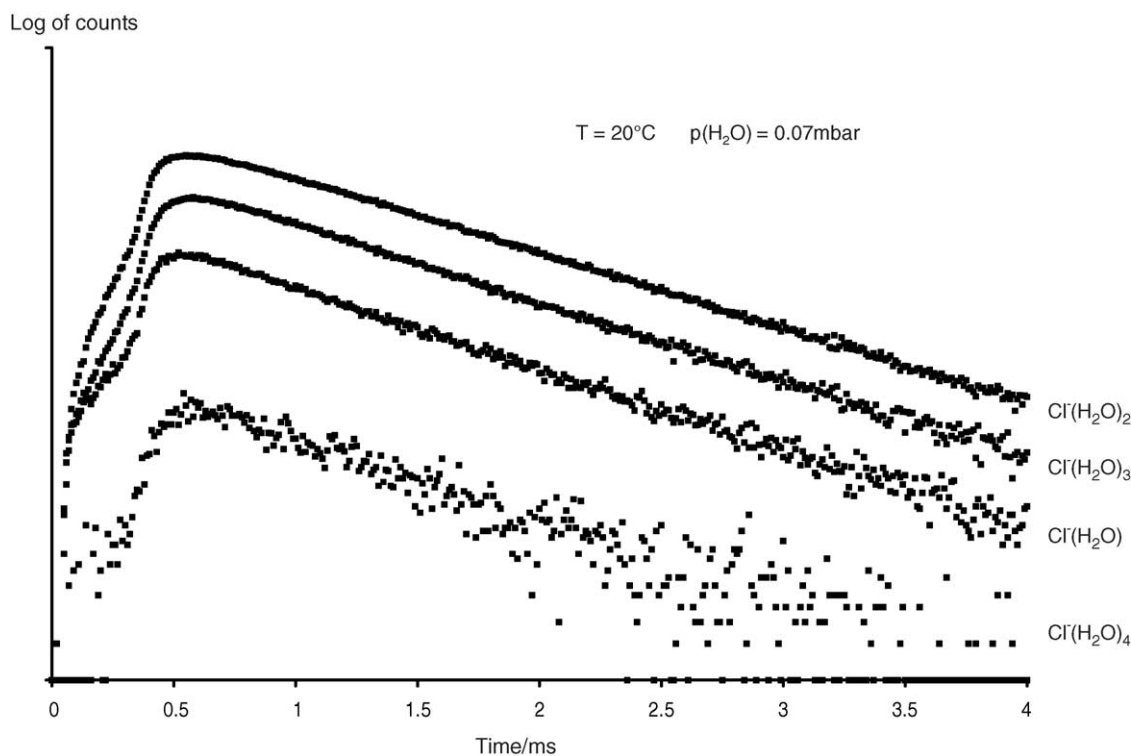


Fig. 5. Some typical chloride ion-water cluster profiles.
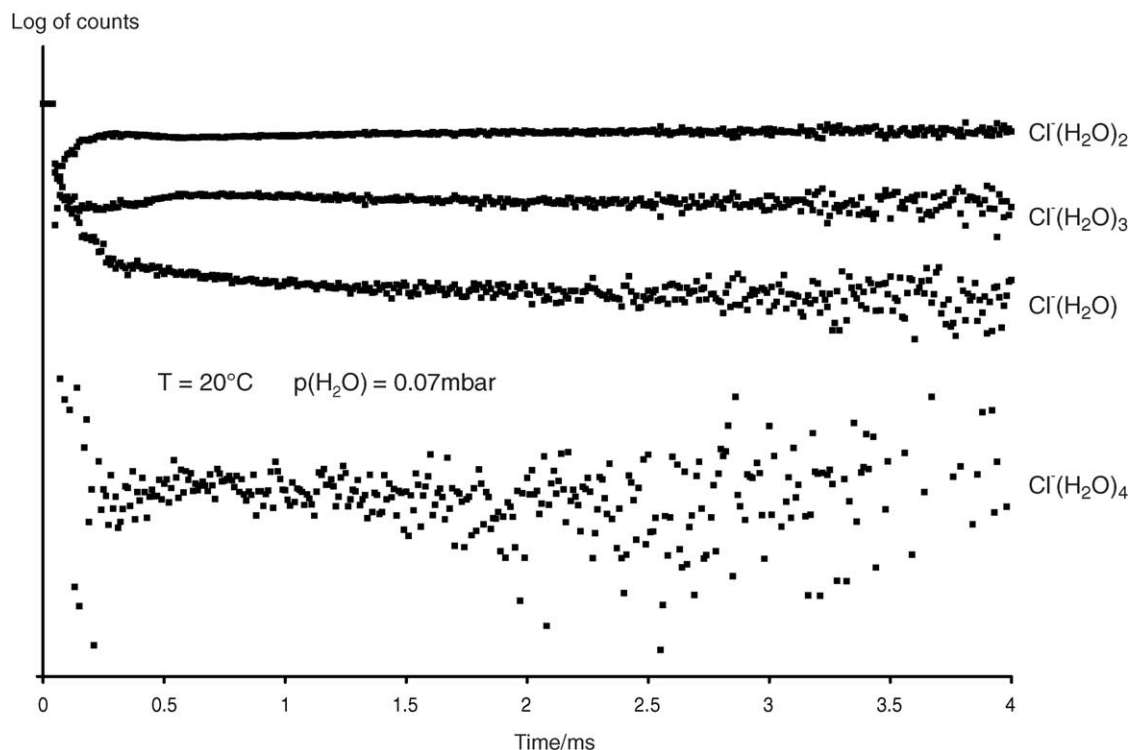
Fig. 6. Hydrated chloride ion profiles as in Fig. 5 but normalized to total ion intensity.

truly parallel and equilibrium is established only about 1.2 ms after the electron beam pulse. Examination of both raw and normalized ionic profiles was used to determine the onset of equilibrium and the time interval over which the ratio of ion intensities should be averaged for calculation of equilibrium constants.

Tests were performed to verify that equilibrium was indeed established by varying the water partial pressure and the total pressure in the ion source. Fig. 7 shows the results of such tests for the (2, 3) hydration step for $Cl^-$. The data points on this plot were obtained not only at different partial pressures of water but also at different total ion source pressures within the ranges shown in Fig. 4.
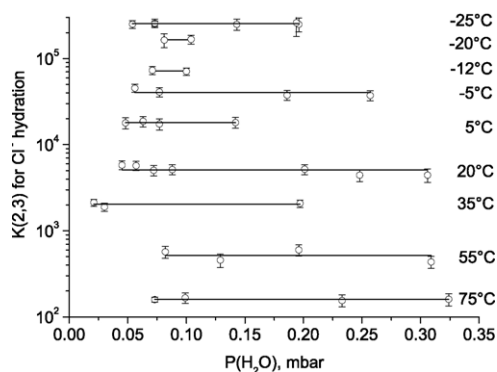


Fig. 7. The equilibrium constant, $K(2, 3)$, as a function of water partial pressure at different temperatures.

Before the experimental results are discussed, it is necessary to review the sources of potential experimental error under certain conditions in the HPMS technique. The expression for the equilibrium constant (3) involves the ratio of ionic abundances and the partial pressure of water in the ion source. Equilibrium constants measured at different temperatures are then used in van't Hoff plots that provide enthalpy and entropy changes for the reaction. Therefore, we will consider factors leading to uncertainties in determination of partial pressure of ligand (water) in the ion source, ionic ratios, and temperature of the reaction.

Errors in the partial pressure of water can arise from errors in ratio of partial pressures of methane and water and errors in measurement of the total ion source pressure, since both these quantities are involved in calculating the partial pressure of water in the ion source. Apart from errors in the sample preparation, errors in the ratio of partial pressures of methane and water might arise from mass discrimination in the neutral gas exiting the ion source [18,19]. It is assumed that the ratio of partial pressures of carrier gas and ligand (methane and water) in the ion source is the same as in the gas handling plant. However, due to mass discrimination there will be an enrichment of the heavier component in the ion source. The maximum magnitude of the enrichment is characterized by the square root of the ratio of masses of water and methane and leads mostly to errors in the entropy, but not the enthalpy. Although this ratio is already close to unity (1.06), the mass discrimination is further reduced by the flow-through design of the ion source. In our experiments, the

ratio of the gas flow into the source to the outflow through the electron entrance and ion exit slits was in the range 1.5–1.8, depending on the source temperature and pressure. In this configuration, errors in the water partial pressure due to mass discrimination of neutral molecules are negligible. Experiments involving heavier ligands should use a carrier gas having a mass close to that of the ligand. Accurate knowledge of the total pressure in the ion source is equally important. Most of HPMS ion source designs follow original designs by Kebarle [1] where the pressure in the ion source is approximated by the pressure in the inlet gas line upstream from the source. Since any gas flow is associated with a pressure drop in the line, the pressure in the ion source is always lower than the upstream pressure. The difference between the two pressures is expected to change monotonically with temperature. This leads to a change in slope of a van't Hoff plot and hence in the calculated enthalpy and entropy of the reaction. The magnitude of the pressure difference will also depend on such factors as the diameter of the gas line, total gas flow, and distance between the ion source and the point where the pressure is actually measured. In our implementation of the HPMS technique, the pressure in the ion source is calculated from the pressures measured upstream and downstream from the source using conductances of the inlet and outlet gas lines and ion source slits calibrated at different ion source temperatures.

Early on in the development of the HPMS technique, problems that affect measured ionic ratios were recognized [20]: (a) adiabatic cooling of the cluster ions following exit from the ion source and non-equilibrium cluster growth, (b) collision-induced dissociation (CID) caused by high gas densities near the ion exit aperture, and (c) unimolecular dissociation of ions during mass analysis. In addition, there are problems associated with mass discrimination in reference to sampling of ions through the ion exit slit as have been discussed in Ref. [5]. Similar to mass discrimination in neutral gas, mass discrimination in ion sampling is characterized by the square root of the ratio of the masses of ions and leads to errors in the entropy, but not the enthalpy. In the case of chloride water clusters, this ratio is not large and the effect of ionic mass discrimination is smaller than experimental errors.

Adiabatic cooling is avoided by ensuring that molecular flow occurs through the ion exit slit that requires a slit width to be smaller than the mean free path of ions under the appropriate experimental conditions. The implementation of molecular flow also reduces collision-induced dissociation, although, CID will always occur to some extent. The number of gas molecules leaving the ion source at any time is considerably larger than the number of exiting ions. A weak electric field is always present outside the source that draws ions into the acceleration section of the mass spectrometer. Some of the ions will inevitably collide with the neutral gas molecules. Due to the requirement of energy and momentum conservation, the maximum energy (of an ion colliding with a gas molecule) available to overcome the energy barrier for

dissociation is limited to,

$$E = eV \frac{m_{\text{gas}}}{m_{\text{ion}} + m_{\text{gas}}} \tag{5}$$

where $eV$ is the kinetic energy of the ion acquired by moving through a potential difference $V$. Evaluation of Eq. (5) with $m_{\text{ion}} = 50$, $m_{\text{gas}} = 16$ (methane), and the typical ion-water clustering reaction value for the dissociation threshold of $45 \, \text{kJ mol}^{-1}$, shows that only 1.8 V acceleration is required for the ion to acquire enough energy to achieve dissociation. The effect of CID on van't Hoff plots has been examined previously [4]. Here the derivation of a more complete expression for the effects of CID on observed equilibrium constants will be given. This derivation considers not only the effect of the degree of dissociation but also the partial pressures of the neutral clustering ligand.

Some simplifying assumptions are required and the accuracy of these will be discussed later. We assume that a fraction, $\alpha$, of ions that dissociate collisionally is identical for $n$ and $n-1$ clusters. The second assumption is that all dissociation occurs before the ions are appreciably accelerated. For this case, dissociating $n+1$ and $n$ clusters will be detected as $n$ and $n-1$, respectively. If the second assumption is invalid, then ions that dissociate after acquiring considerable kinetic energy will not be detected if an electrostatic analyzer is present in the system, as the ESA will energy filter these ions. In the absence of an electrostatic analyzer, the dissociated ions will be detected at different nominal masses, not corresponding to the mass of any of the cluster ions. The third assumption is that $\alpha$ is independent of the internal energy of the ions that is defined by the ion source temperature. Recalling that $n-1$ clusters dissociate to $n-2$ clusters, Eq. (3) can be rewritten as,

$$K_{n,\text{obs}} = \frac{1000[(1-\alpha)I_n + \alpha I_{n+1}]}{p(\text{H}_2\text{O})[(1-\alpha)I_{n-1} + \alpha I_n]} \tag{6}$$

where $K_{n,\text{obs}}$ is the observed equilibrium constant. After algebraic rearrangement and substitution of the relevant equilibrium constants defined by Eq. (3), Eq. (6) becomes

$$K_{n,\text{obs}} = \frac{1000(1-\alpha) + \alpha K_{n+1} p(\text{H}_2\text{O})}{\alpha p(\text{H}_2\text{O}) + 1000/K_n} \tag{7}$$

Now the manner in which the partial pressure of ligand and the degree of dissociation will affect the measured equilibrium constants and hence, the van't Hoff plots, can be explored. Figs. 8 and 9 show how the observed equilibrium constant for the Cl⁻ (2, 3) hydration step differs from the true equilibrium constant at high and low temperatures as a function of $\alpha$ and the partial water vapor pressure. The minimum value for $\alpha$ used in these plots was 0.001. It can be clearly seen that, for $\alpha > 0$, the equilibrium constant rapidly decreases with increasing partial pressure of ligand. The decrease is much larger at low temperatures (Fig. 9) where larger clusters are normally present. Therefore, measurements of larger clusters are much more prone to errors resulting from CID than are measurements of smaller clusters.
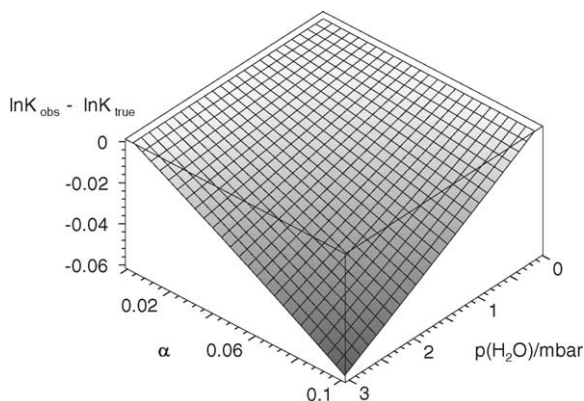
Fig. 8. The effect of collision-induced dissociation on $K(2, 3)$ for $Cl^-$ hydration at $t = 75\,°C$.
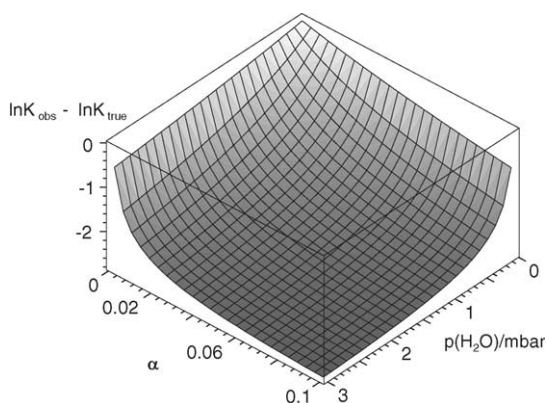


Fig. 9. The effect of collision-induced dissociation on $K(2, 3)$ for $Cl^-$ hydration at $t = -25\,°C$.

Fig. 10 shows a family of van't Hoff plots for the same reaction calculated at a fixed water partial pressure. This figure demonstrates that if measurements are taken over a sufficiently narrow temperature range, a curved van't Hoff
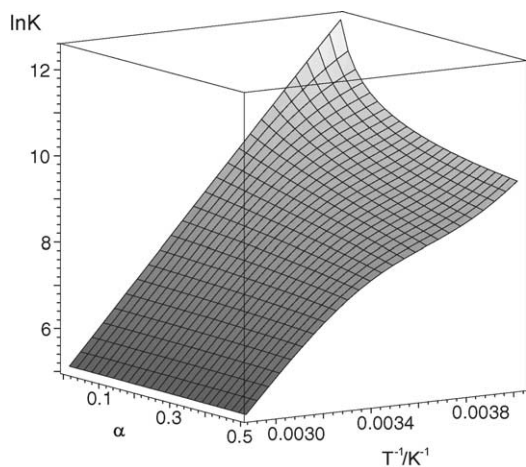


Fig. 10. A family of van't Hoff isochore plots for $K(2, 3)$ for $Cl^-$ hydration at $p(H_2O) = 0.2$ mbar.

plot can be mistaken for a linear one which would lead to smaller absolute values of calculated enthalpy and entropy changes for the studied reaction. If the degree of CID is high enough ($\alpha \geq 0.3$), the plots have inflection points. Experimental scatter of measured equilibrium constants at different temperatures naturally makes it more difficult to distinguish CID.

The equilibrium constants shown in Fig. 7 reveal a tendency to decrease with increasing partial pressure of water vapor. A similar tendency was observed for other reactions measured using our HPMS instrument. If the reason for this behavior was CID, then values of $\alpha$ calculated from these results should be in the range 0.04–0.15 for different ion source pressures. However, van't Hoff plots with these values of $\alpha$ would have considerable curvature at low temperature that was not observed for our experimental results. In addition, a linear dependence of calculated values of $\alpha$ on the ion source pressure was not observed, as would be expected from the argument that $\alpha$ should be proportional to the gas number density outside the source, and, therefore, pressure inside the source. It was found that errors in our calculation of the ion source pressure were the cause of the observed behavior. The ion source pressure in our instrument is calculated from the pressures measured at both ends of the gas inlet and outlet line, whose conductances were calibrated together with the conductance of the source slits. The error in the calculated ion source pressure depends monotonically on the overall pressure, and is still within the assigned accuracy of the calibration (0.05 mbar). This was verified by back-calculating one pressure from the other for each pair of pressures used for the calibration.

The above analysis of CID is somewhat simplified and contains various assumptions. The CID phenomenon, however, is much more complex. The degree of dissociation, $\alpha$, is higher for larger clusters and also increases with the internal energy of clusters determined by the ion source temperature [21]. The full analysis of the effect of CID on van't Hoff plots is rather complicated and will depend on exact experimental conditions used to obtain each equilibrium constant. However, one important result is that HPMS measurements should be undertaken at the lowest possible partial pressures of clustering ligand and overall ion source pressures, as well as an extremely high vacuum in the analyzer. We tried to follow these guidelines in our experiments and the results so obtained do not seem to be affected by CID to any appreciable extent.

The problem of unimolecular dissociation has been previously considered in great detail [22]. Ions leaving the ion source have a thermal energy distribution corresponding to the temperature of the ion source that is not preserved in vacuum due to the absence of thermalizing collisions. The energy stored in activated vibrational and rotational energy levels can be used to overcome the dissociation barrier. The fraction of ions that will have enough energy to exceed the threshold energy for unimolecular dissociation is denoted $f_{ex}$. Depending on the rate constant for unimolecular dissociation

at the temperature of the distribution, a larger or smaller part of that fraction will dissociate during the time required for mass analysis.

Once vibrational frequencies and moments of inertia of a cluster are known, the excited fraction, $f_{ex}$, can be calculated [22], i.e.,

$$f_{ex} = 1 - \frac{1}{Q} \sum_{E_i=0}^{\Delta H} P(E_i) \exp\left(\frac{-E_i}{kT}\right) \qquad (8)$$

where $\Delta H$ for the cluster formation reaction approximates the threshold energy, $Q$ the partition function, and $P(E_i)$ the multiplicity of the state with energy $E_i$. Zero-point energy is the reference energy level. Because of the requirement for angular momentum conservation, the overall rotations were assumed to be unable to provide energy for dissociation. As such, only vibrational frequencies were used in energy calculations and sums of states. These calculations were performed for all chloride water clusters measured experimentally. Experimental measurements were done at sufficiently low temperatures such that $f_{ex}$ did not normally exceed 0.01. The only exception was the (7, 8) hydration step for $Cl^-$. Even at $-80\,°C$ the excited fraction for $Cl^-$ cluster with eight water molecules was calculated to be 0.05. Therefore, we used calculated excited fraction, $f_{ex}$, to correct measured ionic ratios for this step. The rigorous method to correct for unimolecular dissociation is to first calculate unimolecular dissociation rate constants from the Rice–Ramsperger–Kassel–Marcus (RRKM) theory [23], and use these results to calculate the fraction of $f_{ex}$ that will dissociate during mass analysis. Such calculations were reported by Sunner and Kebarle [22]. However, for these calculations assumptions regarding the properties of the activated complex involved in the dissociation reaction, and in particular its vibrational and rotational states, must be made. This and the use of RRKM theory would introduce errors in addition to the errors in the calculated vibrational frequencies and moments of inertia. For simplicity, it was assumed in our calculations that the entire excited fraction, $f_{ex}$, dissociates during mass analysis and the majority of dissociating ions does so only after the acceleration and is rejected by the mass analyzer that includes an ESA in our case. The errors in the corrected ionic ratio due the above assumptions partially cancel. In addition, the estimated difference between the correction involving only $f_{ex}$ and the correction calculated using unimolecular dissociation rate constants [22] was comparable to observed experimental errors.

Errors in measurements of equilibrium ionic ratios and ligand partial pressure leading to errors in calculated equilibrium constants at a given temperature have been discussed. Another source of experimental error in calculated enthalpy and entropy changes for clustering reactions are errors in temperature measurement. Here we consider two cases: (a) errors associated with a temperature sensor itself and (b) errors in measuring the reaction temperature. Previous studies using HPMS, normally had temperature measured using a thermocouple, often not calibrated against any temperature standard.

When resistance of our ion source PRT was converted to temperature using the manufacturer's conversion tables, the discrepancy between this obtained value and the value from our own calibration data was as large as 10 degrees at 600 K. This stresses the importance of performing a rigorous calibration of the temperature sensor. In addition, there is always the question of whether a temperature sensor actually measures true experimental temperature of a reaction. In HPMS experiments, a preheated gas mixture is allowed to flow through the ion source. A common HPMS ion source design incorporates a massive stainless steel block and the temperature measured close to the reaction chamber inside the block is taken to be equal to the experimental temperature of the ion source gas. It is possible and indeed probable that the temperature of the gas inside a reaction chamber of such design differs from the temperature measured by a thermocouple when ion source temperatures are markedly different from the temperature of the preheated gas. This is especially so if the whole source block material is a poor thermal conductor such as stainless steel. The real temperature of the experiment in this case will be closer to the temperature of the preheated gas entering the source than to the temperature measured by a thermocouple.

Fig. 11 shows the dramatic effect that temperature measurement error has on calculated enthalpy changes for two hypothetical reactions with true enthalpy changes having typical values of $48\,kJ\,mol^{-1}$ and measured over the temperature ranges 240–300 and 300–450 K. It was assumed that no temperature measurement error exists at 300 K, and that true experimental temperatures at 240 and 450 K were closer to 300 K than the measured temperatures, 240 and 450 K. As shown in Fig. 11, uncertainties in temperature measurement introduce large errors in calculated enthalpy and entropy changes for these hypothetical reactions. It should be noted that the difference in temperature of gas in the reaction chamber and the source block, if it exists, is expected to become larger at low temperatures because thermal veloc-
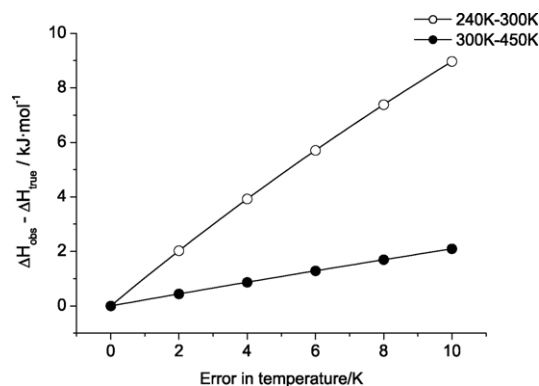


Fig. 11. Effects of temperature errors on resultant enthalpy changes for two reactions measured over the temperature ranges indicated; it is assumed that there is no temperature error at 300 K and that the true experimental temperatures at 450 and 240 K are closer to 300 K than measured by the value plotted on the horizontal axis.
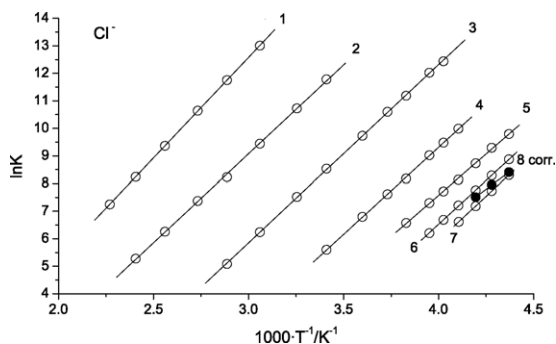
Fig. 12. Experimental van't Hoff isochore plots for $Cl^-$ water clusters; the last hydration step ($n = 8$) is shown with unimolecular dissociation correction applied.

Table 1
Experimentally determined values for $-\Delta H^\circ_{n-1,n}$ [kJ mol$^{-1}$] and $-\Delta S^\circ_{n-1,n}$ [J mol$^{-1}$ K$^{-1}$] for stepwise chloride hydration reactions

| $n$ | $-\Delta H^\circ_{n-1,n}$ | $-\Delta S^\circ_{n-1,n}$ |
|---|---|---|
| 1 | $60.7 \pm 2.1$ | $77.5 \pm 6.3$ |
| 2 | $53.6 \pm 1.3$ | $85.5 \pm 5.0$ |
| 3 | $53.8 \pm 1.7$ | $112.7 \pm 5.9$ |
| 4 | $52.5 \pm 1.7$ | $132.6 \pm 6.3$ |
| 5 | $49.7 \pm 2.1$ | $136.0 \pm 7.5$ |
| 6 | $52.7 \pm 2.5$ | $156.6 \pm 8.4$ |
| 7 | $53.3 \pm 2.5$ | $163.9 \pm 8.4$ |
| 8 | $42.5 \pm 5.0$ (49.8) | $116 \pm 17$ (152) |

Standard pressure is 1000 mbar. Values in parenthesis were calculated from data not corrected for unimolecular dissociation.

ities become smaller and gas densities higher. Under these conditions, longer times are required for the gas to cool down to the temperature of the surrounding ion source block. Fig. 11 also demonstrates that errors in temperature measurement introduce larger errors in measurements of higher solvation steps, since they are carried out at lower temperatures.

Our ion source itself is a very small thin-walled stainless steel spool embedded in a massive copper block. The gas inlet and outlet lines are buried in the block over a distance of approximately 10 cm immediately adjacent to the source. This should ensure that gas entering and leaving the ion source has the same temperature as the ion source itself. The temperature was determined using a four-wire resistance method for the PRT embedded directly in the source gas.

The results for experimentally measured equilibrium constants for $Cl^-$ stepwise hydration reactions are presented in several van't Hoff plots shown in Fig. 12. Two additional solvation steps beyond ones previously measured was directly achieved, as opposed to Ref. [10], where equilibrium constants for those reactions were measured at only one or two temperatures and enthalpy changes were calculated using assumed values for the entropy change. As mentioned previously, the last measured hydration step for $Cl^-$ was corrected for unimolecular dissociation using the theoretically calculated excited fraction. As can be seen in Fig. 12, all data in the van't Hoff plots are linear and no curvature can be distinguished within the experimental scatter. Therefore, enthalpy and entropy changes for halide stepwise hydration reactions calculated from van't Hoff plots and given in Table 1 are independent of temperature within the observed experimental errors. Errors due to mass discrimination in ion sampling, as mentioned above, are small compared with experimental errors and, therefore, entropies were not corrected for mass discrimination.

Equilibria containing higher ligand numbers cannot be measured accurately with the present HPMS method. Observation of such equilibria would require low temperatures and high water partial pressures in the source. There is a lower boundary temperature below which experimentally usable data cannot be obtained as water begins to condense in the ion source when its pressure becomes equal to the saturated

water vapor pressure at that temperature. We observed such condensation at $-45\,^\circ$C. Increasing the water partial pressures at higher temperatures will allow observation of larger clusters. However, at high temperatures, a significant fraction of large clusters will undergo undesirable unimolecular dissociation during mass analysis and even though measured ionic ratios could be corrected theoretically, such results would be of significantly lower accuracy. In addition to the uncertainty of the unimolecular dissociation correction, the use of high water partial pressures would strongly enhance the collision induced dissociation effect on measured ionic ratios as was shown previously in Figs. 8 and 9. The effect of CID is more difficult to estimate quantitatively and the accuracy of the ionic ratios corrected for both unimolecular dissociation and CID would be even lower.

Comparisons of our data with previous experimental results and DFT calculations are shown in Figs. 13 and 14. There is obvious disagreement between the present results and earlier experimental data for higher hydration steps, but good agreement with DFT calculations, especially for the stepwise trends in enthalpy and entropy changes. Results for enthalpies are shifted upward compared with previous results and exhibit non-monotonic dependence with cluster size. The upward shift may be a result of uncertainties in reaction tem-
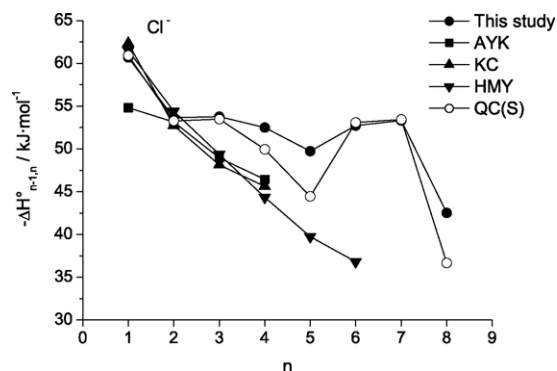


Fig. 13. Comparison of enthalpy changes for $Cl^-$ hydration reactions obtained in this work with previous data and calculations; AYK—data from Ref. [12], KC—data from Ref. [11], HMY—data from Ref. [10], QC(S)—DFT calculation; the last hydration step ($n = 8$) is shown with unimolecular dissociation correction applied.
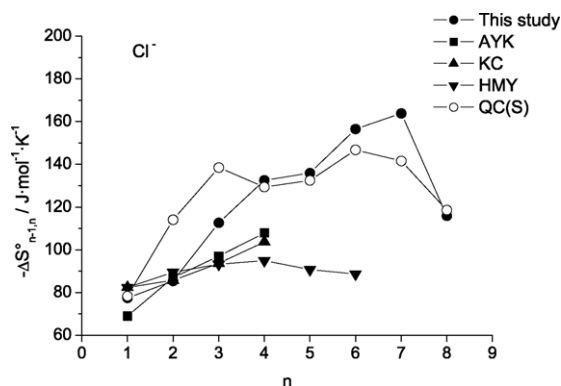
Fig. 14. Comparison of entropy changes for $Cl^-$ hydration reactions obtained in this work with previous data and calculations; AYK—data from Ref. [12], KC—data from Ref. [11], HMY—data from Ref. [10], QC(S)—DFT calculation; the last hydration step ($n = 8$) is shown with unimolecular dissociation correction applied.

perature or ion source pressure measurement in earlier HPMS designs. The disagreement is largest for reactions measured at low temperatures, which is consistent with the assumption of temperature measurement errors as is shown in Fig. 11 or earlier discussion of ion source pressure errors. In addition to the above factors, a smaller contribution to the differences between present and earlier data might arise from possible CID problems in previous determinations. Ion source pressures of 3–4 Torr cited in Refs. [10–12] might be too high for measurements at low temperatures. For comparison, pressure ranges used at different temperatures in our experiments are shown in Fig. 4. The appearance of the non-monotonic trends in our results is attributed in part to an improved energy resolution in the present HPMS setup. This is a result of an increased sensitivity of the mass spectrometer due to higher acceleration voltages, improved ion optics, and the use of a data system for unambiguous and repeatable mass tuning combined with the possibility to quickly switch between different masses several times in the course of one measurement.

Water molecules in halide water clusters are attached to the anion and other water molecules through hydrogen bonds. As a result, ion-solvent and solvent-solvent interactions in these clusters can be approximately of the same magnitude. Non-monotonic dependence of stepwise thermochemical values on cluster size demonstrates the competition between these two types of interactions. Such trends were also observed in studies of hydration of other halides that have been performed using our HPMS apparatus. Results of those experiments, corresponding DFT calculations, and interpretation of the stepwise behavior of enthalpies and entropies of hydration of $Cl^-$, $Br^-$, and $I^-$ will be reported elsewhere [24].

## Acknowledgements

## References

[1] P. Kebarle, in: J.M. Farrar, W. Saunders Jr. (Eds.), Techniques for the Study of Ion-Molecule Reactions, Wiley, New York, 1988.

[2] K. Hiraoka, K. Morise, T. Nishijima, S. Nakamura, M. Nakazato, K. Ohkuma, Int. J. Mass Spectrom. Ion Process. 68 (1986) 99.

[3] J.E. Szulejko, J.J. Fisher, T.B. McMahon, J. Wronka, Int. J. Mass Spectrom. Ion Process. 83 (1988) 147.

[4] K. Hiraoka, P. Kebarle, J. Am. Chem. Soc. 97 (1975) 4179.

[5] J.K. Hovey, A. Likholyot, Int. J. Mass Spectrom. 202 (2000) 147.

[6] J.E. Szulejko, C.E.C.A. Hop, T.B. McMahon, A.G. Harrison, A.B. Young, J.A. Stone, J. Am. Soc. Mass Spectrom. 3 (1992) 33.

[7] SIMION, http://www.inel.gov/env-energyscience/chemistry/simion-software.shtml.

[8] X. Chen, L. Oscarson, H. Cao, S.E. Gillespie, R.M. Izatt, Thermochim. Acta 285 (1996) 11.

[9] B.W. Mangum, G.T. Furukawa, Guidelines for realizing the ITS-90, in: NIST Technical Note 1265, National Institute of Standards, 1990.

[10] K. Hiraoka, S. Mizuse, S. Yamabe, J. Am. Chem. Soc. 92 (1988) 3943.

[11] R.G. Keesee, A.W. Castleman Jr., Chem. Phys. Lett. 74 (1980) 139.

[12] M. Arshadi, R. Yamadagni, P. Kebarle, J. Phys. Chem. 74 (1970) 1475.

[13] M.J. Frisch, G.W. Trucks, H.B. Schlegel, G.E. Scuseria, M.A. Robb, J.R. Cheeseman, V.G. Zakrzewski, J.A. Montgomery, R.E. Stratmann, J.C. Burant, S. Dapprich, J.M. Millam, A.D. Daniels, K.N. Kudin, M.C. Strain, O. Farkas, J. Tomasi, V. Barone, M. Cossi, R. Cammi, B. Mennucci, C. Pomelli, C. Adamo, S. Clifford, J. Ochterski, G.A. Petersson, P.Y. Ayala, Q. Cui, K. Morokuma, D.K. Malick, A.D. Rabuck, K. Raghavachari, J.B. Foresman, J. Cioslowski, J.V. Ortiz, B.B. Stefanov, G. Liu, A. Liashenko, P. Piskorz, I. Komaromi, R. Gomperts, R.L. Martin, D.J. Fox, T. Keith, M.A. Al-Laham, C.Y. Peng, A. Nanayakkara, C. Gonzalez, M. Challacombe, P.M.W. Gill, B. Johnson, W. Chen, GAUSSIAN 98, Revision A.6, Gaussian Inc., Pittsburgh, PA, 1998.

[14] J.E. Combariza, N.R. Kestner, J. Jortner, Chem. Phys. Lett. 203 (1992) 423.

[15] J.E. Combariza, N.R. Kestner, J. Jortner, J. Chem. Phys. 100 (1994) 2851.

[16] R. Ayala, J.M. Martinez, R.R. Pappalardo, E.S. Marcos, J. Phys. Chem. 104 (2000) 2799.

[17] A. Good, D.A. Durden, P. Kebarle, J. Chem. Phys. 52 (1970) 212.

[18] D.S. McGrew, W.B. Knighton, J.A. Bognar, E.P. Grimsrud, Int. J. Mass Spectrom. Ion Process. 139 (1994) 47.

[19] D.H. Williamson, W.B. Knighton, E.P. Grimsrud, Int. J. Mass Spectrom. Ion Process. 154 (1996) 15.

[20] A.M. Hogg, P. Kebarle, J. Chem. Phys. 43 (1965) 449.

[21] Y.K. Lau, S. Ikuta, P. Kebarle, J. Am. Chem. Soc. 104 (1982) 1462.

[22] J. Sunner, P. Kebarle, J. Phys. Chem. 85 (1981) 327.

[23] R.A. Markus, J. Chem. Phys. 20 (1952) 359.

[24] A. Likholyot, J.K. Hovey, T.M. Seward, Geochim. Cosmochim. Acta 69 (2005), in press.